High-Resolution Plant Shape Measurements from Multi-View Stereo Reconstruction

Maria Klodt and Daniel Cremers

Technische Universität München

Abstract. Accurate high-resolution 3D models are essential for a non-invasive analysis of phenotypic characteristics of plants. Leaf surface areas, fruit volumes and leaf inclination angles are typically of interest. This work presents a globally optimal 3D geometry reconstruction method that is specialized to high-resolutions and is thus suitable to reconstruct thin structures typically occuring in the geometry of plants. Volumetric 3D models are computed in a convex optimization framework from a set of RGB input images depicting the plant from different view points. The method uses the memory and run-time efficient octree data structure for fast computations of high-resolution 3D models. Results show accurate 3D reconstructions of barley, while an increase in resolution of a factor of up to 2000 is achieved in comparison to the use of a uniform voxel based data structure, making the choice of data structure crucial for feasible resolutions.

Keywords: Stereo Reconstruction; Convex Optimization; Plant Phenotyping; Octrees

1   Introduction

Plant phenotyping increasingly relies on precise 3D models of plants, demanding for automated and accurate reconstruction methods specialized for plant geometry. Applications include the determination of volume and surface dimensions, leaf quantification, and leaf inclination angles [28]. These applications share the benefit from accurate high-resolution 3D plant models. Since manual examination of phenotypic characteristics is usually time consuming and destructive, non-invasive and automated methods are needed for high-throughput applications and monitoring of specimen over time.

Convex optimization methods provide a powerful technique for inferring the 3D structure of an object from a set of images in a globally optimal way [16]. Volumetric methods as used in [16, 11] allow for reconstructions of dense surfaces, at limited resolution due to large memory requirements of the underlying data structures. Point cloud reconstructions from images as used in [9] require less memory while neglecting density.

3D reconstruction of plants requires special consideration to the fine scaled features typically occuring in plant geometry. The usual assumption that the

object to reconstruct is compact does not apply. Reconstruction of thin structures based on silhouette constraints as proposed in [6] allows to preserve fine structures while the uniform voxel based data structure still limits the resolution. For thin objects volumetric approaches yield large amounts of empty space, implying the need for more efficient non-uniform data structures.

Originally introduced for computer graphics, octrees [23] provide a memory-efficient data structure for large scale 3D objects. Large-scale reconstructions for fusion of RGB-D images into a volumetric model have shown that an octree based data structure avoids memory limitations in 3D reconstructions [31]. A non-hierarchical memory-efficient approach for volumetric representations is the narrow band method. Narrow bands for 3D reconstruction in graph cuts have been presented in [18].

Full 3D shape measurements of plants allow for a variety of phenotypic applications. However, phenotyping is a major bottleneck in crop plant research [14], which strongly benefits of automated approaches especially when dealing with large datasets. A special importance lies on high-resolution reconstruction of plant shapes for a better comprehension of phenotypes [7]. Laser scanners are a capable tool for the aquisition of high-precision 3D point clouds of plants [21], however provide no volumetric and surface area information. Time-of-flight cameras and RGB-D sensors like the *Kinect* capture 3D information at a lower resolution. They are also used in agriculture however are known to be less robust to bright illumination than stereo vision [1, 13]. In the last years, image analysis has become a widely used technique for non-invasive methods for plant phenotyping [8]. Applications include the monitoring of growth rates which can be used as a measure for drought tolerance of wheat and barley [25], classification of leaves and stems [26], or computation of leaf inclination angles [3]. In [29] an image based method for 4D reconstruction of plants based on optical flow is introduced. Another application is the determination of the leaf canopy area from images [19], an ecological indicator variable whose estimation usuallly is laborious [17].

This work presents a novel method for volumetric 3D reconstruction of plants from a set of RGB images, specialized on accuracy and high-resolution. The method is implemented in a convex framework allowing for global optimization of the chosen model which makes it independent of initializations. The underlying data structure is based on octrees, which enable a fast and memory-efficient implementation, making high resolutions possible. In this work we show that the choice of data structure is not only beneficial for reducing run-time and memory requirements, but crucial to make high-resolutions possible.

Fig. 1 shows results of the proposed method for a 3D reconstruction of barley. For a plant of 10 cm height a resolution of $1.8 \cdot 10^{-6}$ mm^3 is achieved by the use of an octree data structure. The use of octrees enables a more than 2000 times higher resolution compared to a uniformely spaced voxel grid using the same amount of memory. Especially in the case of thin structures, the data structure is critical to avoid memory limitations.

(a) 4 of 25
Input Images

(b) Camera
Positions

(c) Reconstructed
3D Model
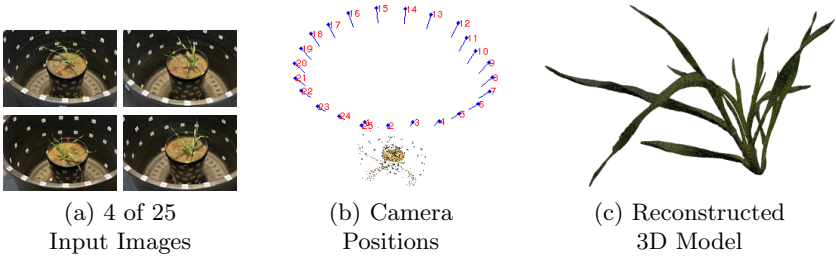
Fig. 1. 3D-Reconstruction of a barley, computed from 25 input images. The reconstructed 3D model consists of $\sim$12 million octree nodes.

2   High-Resolution Stereo Reconstruction with Octrees

We consider a continuous image domain $\Omega \subset \mathbb{R}^2$. Given a set of m input images $I_1, \ldots, I_m : \Omega \to \mathbb{R}$ depicting the object from different view points, we compute a surface $\Sigma \subset \mathbb{R}^3$ that gives rise to the images. To reconstruct a full 3D model, each object point must be visible in at least two images. Fig. 1 (b) shows an example for 25 camera positions, computed with software of [22] and [30].

The surface is optimized inside the visual hull [20] $\mathcal{H} \subset \mathbb{R}^3$ which is determined by silhouette images. The silhouette images $S_i : \Omega \to \{0, 1\}, i = 1, \ldots m$ are defined as $S_i(p) = 1$ at points $p \in \Omega$ that depict the plant and $S_i(p) = 0$ otherwise, i.e. at points that depict background. We compute silhouette images using an interactive image segmentation method [33]. The visual hull is the smallest volume whose projections to the input images cover the silhouettes of the object.

We propose the use of volume constraints to ensure a stable substance of the reconstructed object. Volume constraints have been proposed for single view reconstruction [32] and image segmentation [15, 10].

2.1   Surface Optimization with Volume Constraints

The surface Σ is represented implicitly by an indicator function $\mathbf{1}_\Sigma : \mathcal{H} \to \{0, 1\}$ that defines a segmentation of the volume enclosed by $\mathcal{H}$ to plant, i.e. $\mathbf{1}_\Sigma(x) = 1$, and background, i.e. $\mathbf{1}_\Sigma(x) = 0$. Relaxing the domain to the continuous domain $[0, 1]$ allows for convex optimization of the corresponding segmentation $u : \mathcal{H} \to [0, 1]$. We consider the following convex optimization problem

$$\min_u \left\{ \int_\mathcal{H} g(x) \left| \nabla(u) \right| + \lambda \int_\mathcal{H} f(x) u(x) \, \mathrm{d}x \right\}, \quad \text{s.t.} \quad \mathcal{V}(u) \geq c, \qquad (1)$$

where $\mathcal{V}$ refers to the volume of the object, i.e.

$$\mathcal{V}(u) = \int_\mathcal{H} u(x) \, \mathrm{d}x. \qquad (2)$$

and $c \in \mathbb{R}$ is the minimum volume. In the experiments shown in this paper, the volume constraint parameter was set to $c = 0.9 \cdot |\mathcal{H}|$ which implies that the

volume of the segmented object should be at least 90% of the volume enclosed
by the visual hull. The data term $f : \mathcal{H} \to \mathbb{R}$, weighted with $\lambda \in \mathbb{R}$, implements
the assumption that the visual hull is a rough estimator for the object and is
based on the distance of a point to the border $\partial \mathcal{H}$ of the domain:

$$f(x) = 1 - \min_{\hat{x} \in \partial \mathcal{H}} \| x - \hat{x} \| . \tag{3}$$

For the m input images $I_1, \ldots, I_m : \Omega \to \mathbb{R}$ the photoconsistency g is com-
puted as the intensity difference of the best matching image pair:

$$g(x) = \min_{i,j \in \{1,\ldots,m\}, i \neq j} (|I_i(\pi_i(x)) - I_j(\pi_j(x))|), \tag{4}$$

where $\pi_i : \mathbb{R}^3 \to \Omega$ is the projection of a 3D point x to image I_i. $g(x)$ is used as
a weighting function for the gradient norm $|\nabla(u)|$, directing the surface through
points whose projections to the images have similar intensity.

A minimizer of (1) is computed using a primal-dual optimization [5] scheme
with gradient descent in the primal variable u and gradient ascent in the dual
variable $p : \mathcal{H} \to \mathbb{R}^3$

$$p^{t+1} = \Pi_C \left(p^t + \tau \nabla u^t \right) \tag{5}$$

$$u^{t+1} = \Pi_{\mathcal{V}} \left(u^t + \sigma(\mathrm{div}(p^{t+1}) - \lambda f) \right) \tag{6}$$

and the projections

$$\Pi_C(p) = \frac{p}{\max \left\{ 1, \frac{|p|}{g} \right\}} \tag{7}$$

$$\Pi_{\mathcal{V}}(u) = u + \max \left\{ \frac{1}{|\mathcal{H}|} \left(c - \int_{\mathcal{H}} u(x) \, dx \right), 0 \right\} . \tag{8}$$

The time steps τ and σ were set to $\tau = \sigma = 0.3$. The projection $\Pi_{\mathcal{V}}$ projects the
current u to the volume constraint $\mathcal{V}(u) \geq c$, and is computed analog to the area
constraint in [15]. The projection Π_C was presented in [4]. The boundary con-
ditions are Dirichlet conditions for the gradient, i.e. $\nabla u|_{\partial \mathcal{H}} = 0$, and Neumann
conditions for the divergence, i.e. $\mathrm{div}(p)|_{\partial \mathcal{H}} = p$.

2.2   A Memory-Efficient Data Structure using Octrees

An octree is a tree data structure whose nodes have either eight or no sub nodes.
Nodes with eight sub nodes are denoted as *inner nodes* and nodes without sub
nodes as *leaf nodes*. Octrees provide a memory-efficient data structure for 3D
volumes.

Building the Octree The octree data structure is computed from the silhou-
ette images in a top-down approach starting at a root node enclosing the whole
scene depicted in the images. Subsequently, nodes are subdivided depending on

| Depth 7 | Depth 8 | Depth 9 | Depth 10 | Depth 11 | Depth 13 |
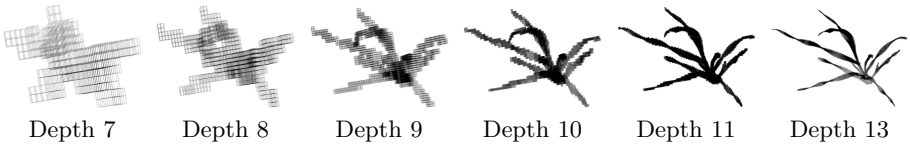
Fig. 2. Octree data structure for increasing resolution, i.e. depth of the tree. The figures show the bounding boxes of all leaf nodes in the deepest level of the octree. The data structure is built in a top-down method where each level is complete in itself but can be refined for higher resolution.

the structure of the visual hull. Fig. 2 shows an example octree at different steps of the iteration.

Each node gets a assigned a bounding cuboid with coordinates $C := (x_{\min}, y_{\min}, z_{\min}, x_{\max}, y_{\max}, z_{\max})$ that define the volume enclosed by the node. The camera positions and viewing angles define a bounding cuboid which define the respective coordinates of the root node. The nodes are subsequently divided into eight sub-nodes of equal size if the visual hull passes the bounding cuboid of the node. The visual hull passes the cuboid if the projection of the cuboid's faces to the images contains both plant and background for at least one of the m input images. The nodes are refined until a predefined maximal depth is reached that corresponds to the desired resolution. In each iteration the octree contains the visual hull in the leaves of the deepest level. Note that it is not necessary that the bounding cuboid is as small as possible since the subsequent subdivision of the data structure will prevent the allocation of too many nodes.

Neighborhood Connectivity of Nodes To compute the derivatives for the gradient and divergence operators in the optimization update steps (5) and (6) each leaf node in the octree requires access to the function values of its neighboring nodes. Each node stores a reference to its parent node, and the inner nodes also to the eight sub nodes. Storing additional references to the six neighboring nodes respectively saves run-time while needing more memory. We compute the neighboring nodes for each node every time when access to it is needed. We chose not to precompute them, because experiments showed that the run-time improvement is not significant. Due to the bounding cuboid each node has defined, neighboring nodes can be found by its coordinates via traversing one path of the tree from the root to the node. The respective run-time is in $O(\log(n))$, where n is the number of nodes in the octree and $\log(n)$ is the maximal depth.

3 Performance Evaluation

We evaluate the method with respect to accuracy and memory requirements for 3D reconstructions of barley.

Fig. 3. Volumetric 3D Reconstruction of a barley, computed from 25 RGB images. The dense surface is optimized in the leaf nodes of deepest level in an octree of depth 14.

3.1   High-Resolution Volumetric 3D Reconstruction of Barley

Fig. 3 shows reconstruction results for barley for the input images shown in Fig. 1(a). The images were captured with a standard consumer camera at a resolution of 5184×3456 pixels. The camera capturing positions were computed using the software of [22] and [30]. The octree that was computed to reconstruct the 3D model has a depth of 14 and its computation took around 30 minutes, making the method suitable for offline reconstructions.

3.2   Accuracy of the Reconstruction

We measure the accuracy of the reconstructed 3D model by projecting its silhouette to the input images and computing the difference to manually segmented ground truth images. Since an objective ground truth in 3D is not available, the projection error is measured in the image domain. Fig. 4 shows that the proposed 3D reconstruction with octrees enables accurate 3D reconstruction of fine-scaled structures of the plant. The figure shows a projection of the reconstructed object to one of the original images. The similarity of the projected silhouette compared to the manually segmented ground truth is 0.96. As similarity measurement the dice coeffient was used, where a value of 1 corresponds

(a) Silhouette Projection	(b) Close-up View 1	(c) Close-up View 2	(d) Close-up View 3
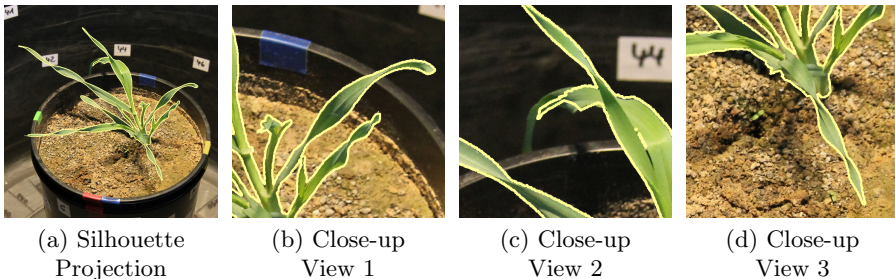
Fig. 4. The high-resolution data structure allows for accurate 3D reconstruction. (a): The silhouette of the reconstructed 3D model is projected to one of the input images. (b-d): Close-up views visualize the accuracy of the reconstruction. The similarity of the projected silhouette compared to the ground truth is 0.96.

	Uniform Grid:		Octree:		
Octree Depth	Number of Voxels	Memory Requirement	Number of Nodes	Memory Requirement	Comparison Factor
7	64^3	1 MB	10^3	85 KB	12
8	128^3	8 MB	$3 \cdot 10^3$	240 KB	34
9	256^3	64 MB	$9 \cdot 10^3$	650 KB	101
10	512^3	512 MB	$27 \cdot 10^3$	1.9 MB	269
11	1024^3	4 GB	$96 \cdot 10^3$	6.6 MB	621
12	2048^3	32 GB	$413 \cdot 10^3$	29 MB	1129
13	4096^3	256 GB	$2 \cdot 10^6$	172 MB	1524
14	8192^3	2 TB	$15 \cdot 10^6$	1 GB	2048

Table 1. Comparison of memory requirements (approximate values) for 3D reconstruction in a uniformly spaced voxel grid versus octree. Memory limits of a current consumer PC are reached for the regular grid already at a resolution of 1024^3, while an octree of depth 14 fits. This makes the octree a suitable data structure for 3D reconstruction of thin structures occuring in plants.

to a perfect overlap and 0 to no overlap. The close-up view in Fig. 4 (c) shows an example where the reconstructed model is inaccurate: the reconstruction does not contain the whole leaf in the middle of the image. In this case this is due to the fact that the leaf is not visible in some of the images and the region is hence segmented as background in 3D.

3.3 Performance Analysis

The memory requirements and resolution of the proposed method are compared to a standard volumetric approach using regular grids. A regular grid is a subdivision of a 3D volume into uniformly sized cuboids, also denoted as voxels. This yields a data volume with large amounts of empty voxels – in contrast to the octree with nodes of different sizes depending on the structure of the shape.

Tab. 1 shows a comparison of memory requirements for the octree data structure and the alternative representation using a regular grid. The values for the uniform grid were computed for each resolution while the values for the octree were measured experimentally for the example 3D model shown in Fig. 3. In each row of the table the actual size of a voxel is the same as the size of an octree node. Due to the connectivity of nodes the memory requirement for a single octree node is higher than the requirement for a single voxel, however the overall memory consumption is significantly reduced. For the uniform grid a resolution of 1024^3 reaches the limit of a current consumer PC with 4 GB RAM. The octree of depth 14 requires 1 GB, corresponding to a voxel volume of 8192^3. For a plant of 10 cm height, an octree node inside the visual hull covers a volume of $1.8 \cdot 10^{-6}$ mm^3, yielding a 2048 times higher resolution than a voxel of the regular grid fitting in the same memory, which covers a volume of 0.0037 mm^3. The experiment shows that the choice of data structure is crucial to make high-resolutions feasible for volumetric reconstructions.

4   3D Plant Shape Models for Phenotyping

Full 3D models of plants allow for phenoypic analysis including the computation of volumes and surface areas or leaf inclination angles. Further analysis like monitoring of plant growth is possible since the plants are not destroyed during the process of reconstruction.

4.1   Measuring Volume and Surface Area

The volume and surface area of a plant are fundamental indicators for growth analysis [27]. Volumetric models have the advantage that precise information on these features can be directly extracted from the shape.

The volume $\mathcal{V}(u)$ measured in voxels can be computed from the segmented surface u using equation (2). To obtain absolute measurements in cm^3, a reference measurement is necessary, for example the overall height h of the plant in cm, or in case of fixed cameras the baselines between the camera optical centers. The absolute volume $V(u)$ of the plant model can then be computed by a respective scaling of $\mathcal{V}(u)$, i.e. with $h^3/2^{3d}$, where d is the depth of the octree. If no reference measurement is given, the volume can be computed up to a constant scalar factor.

The surface area $A(u)$ corresponds to the boundary size of the reconstructed shape and can be computed from u with

$$A(u) = \int_{\mathcal{H}} |\nabla(u)| \, \mathrm{d}x. \tag{9}$$

For the barley shown in Fig. 3 we measured a volume of $V(u) \approx 3.101$ cm^3 and a surface area of $A(u) \approx 106.1$ cm^2 for a plant height of 10 cm.

4.2   Quantification of Leaves

The total leaf number of a plant is an important trait used to monitor vegetative development. It can be used as an indicator to measure influences of drought [12] or to determine flowering times [24].

The full 3D models of plant shapes allow for automated quantification of leaves as the experiment in Fig. 5 shows for a barley. The reconstructed 3D model (Fig. 5 (a)) is segmented into two regions according to the eigenvalues of the second-moments tensor of the surface (Fig. 5 (b)). The 3D second-moments tensor [2] of a shape u is defined as

$$M(u) = \int_{\mathcal{H}} G_\sigma * \nabla u \nabla u^\top \, \mathrm{d}x \tag{10}$$

where G_σ is a gaussian convolution with standard deviation σ. The eigenvalues of M represent the distribution of gradient directions of the shape, and thus provide a robust classifier for a segmentation based on local geometric structures. Due to the high resolution of the 3D model the eigenvalues can be computed precisely. The connected components (Fig. 5 (c)) of the resulting segmentation allow for an automated quantification of leaves.

(a) 3D Model
of a Barley

(b) Segmented
Surface

(c) Connected
Components
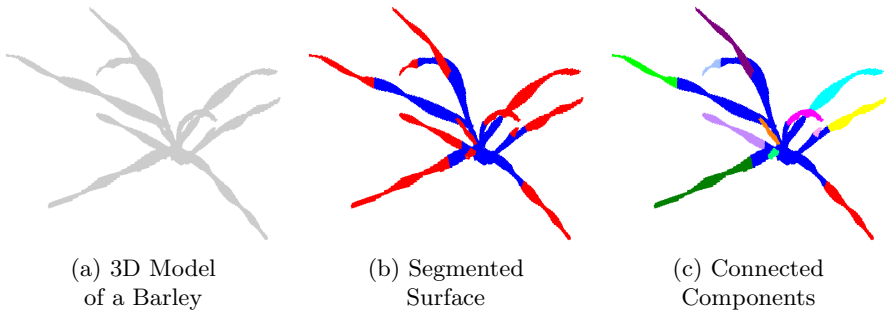
Fig. 5. Segmentation of the 3D surface, based on the eigenvalues of the second-moments tensor. The connected components of the segmentation yield quantitative information like the number of leaves in the plant.

5 Conclusion

We proposed a method for the reconstruction of high-resolution volumetric 3D models of plants from a set of RGB images. The reconstructed full 3D models allow for accurate phenotypic analysis of the geometric properties of plants including volume and surface areas or quantification of leaves. We showed that the octree data structure is especially suitable for volumetric reconstruction of thin features that typically occur in plant geometry. Moreover, we showed that the choice of a suitable data structure is essential to make high-resolution 3D model reconstruction possible. Compared to standard data structures, like regular grids, up to 2000 times higher resolutions are feasible. Possible future work includes a space-time reconstruction of plant growth. The non-invasiveness of the method allows for a monitoring of specimen over a time period.

Acknowledgements

References

1. Abbas, S.M., Muhammad, A.: Outdoor rgb-d slam performance in slow mine detection. In: Robotics; Proceedings of ROBOTIK 2012; 7th German Conference on. pp. 1–6. VDE (2012)
2. Bigün, J., Granlund, G.H.: Optimal orientation detection of linear symmetry. In: IEEE First International Conference on Computer Vision (ICCV). pp. 433–438. London, Great Britain (June 1987)

3. Biskup, B., Scharr, H., Schurr, U., Rascher, U.: A stereo imaging system for measuring structural parameters of plant canopies. Plant Cell Environ 30(10), 1299–308 (2007)

4. Chambolle, A.: Total variation minimization and a class of binary MRF models. In: Int. Conf. on Energy Minimization Methods for Computer Vision and Pattern Recognition. pp. 136–152. No. 3757 in LNCS, Springer (2005)

5. Chambolle, A., Pock, T.: A first-order primal-dual algorithm for convex problems with applications to imaging. Journal of Mathematical Imaging and Vision 40(1), 120–145 (2011)

6. Cremers, D., Kolev, K.: Multiview stereo and silhouette consistency via convex functionals over convex domains. IEEE Transactions on Pattern Analysis and Machine Intelligence 33(6), 1161–1174 (2011)

7. Dhondt, S., Wuyts, N., Inzé, D.: Cell to whole-plant phenotyping: the best is yet to come. Trends in Plant Science 18(8), 433–444 (2013)

8. Fiorani, F., Schurr, U.: Future scenarios for plant phenotyping. Annual review of plant biology 64, 267 – 291 (2013)

9. Furukawa, Y., Ponce, J.: Accurate, dense, and robust multiview stereopsis. IEEE Transactions on Pattern Analysis and Machine Intelligence 32(8), 1362–1376 (2010)

10. Gorelick, L., Schmidt, F.R., Boykov, Y., Delong, A., Ward, A.: Segmentation with non-linear regional constraints via line-search cuts. In: European Conference on Computer Vision (ECCV). Florence, Italy (Oct 2012)

11. Graber, G., Pock, T., Bischof, H.: Online 3d reconstruction using convex optimization. In: 1st Workshop on Live Dense Reconstruction From Moving Cameras, ICCV 2011 (2011)

12. Granier, C., Aguirrezabal, L., Chenu, K., Cookson, S., Dauzat, M., Hamard, P., Thioux, J., Rolland, G., Bouchier-Combaud, S., Lebaudy, A.: Phenopsis, an automated platform for reproducible phenotyping of plant responses to soil water deficit in arabidopsis thaliana permitted the identification of an accession with low sensitivity to soil water deficit. New Phytologist 169, 623–635 (2006)

13. Kazmi, W., Foix, S., Alenya, G., Andersen, H.J.: Indoor and outdoor depth imaging of leaves with time-of-flight and stereo vision sensors: Analysis and comparison. ISPRS Journal of Photogrammetry and Remote Sensing 88(0), 128 – 146 (2014)

14. Kilian, B., Graner, A.: Ngs technologies for analyzing germplasm diversity in genebanks. Brief Funct Genomics 11(1), 38–50 (Jan 2012)

15. Klodt, M., Cremers, D.: A Convex Framework for Image Segmentation with Moment Constraints. In: IEEE International Conference on Computer Vision (ICCV) (2011)

16. Kolev, K., Klodt, M., Brox, T., Cremers, D.: Continuous Global Optimization in Multiview 3D Reconstruction. International Journal of Computer Vision (IJCV) 84(1), 80–96 (August 2009)

17. Korhonen, L., Heikkinen, J.: Automated Analysis of in Situ Canopy Images for the Estimation of Forest Canopy Cover. Forest Science 55(4), 323–334 (Aug 2009)

18. Ladikos, A., Benhimane, S., Navab, N.: Multi-view reconstruction using narrow-band graph-cuts and surface normal optimization. In: BMVC. pp. 1–10 (2008)

19. Lati, R.N., Filin, S., Eizenberg, H.: Robust methods for measurement of leaf-cover area and biomass from image data. Weed Science 59(2), 276–284 (April-June 2011)

20. Laurentini, A.: The visual hull concept for silhouette-based image understanding. IEEE Trans. Pattern Anal. Mach. Intell. 16(2), 150–162 (Feb 1994)

21. Louarn, G., Carré, S., Boudon, F., Eprinchard, A., Combes, D.: Characterization of whole plant leaf area properties using laser scanner point clouds. In: Fourth

International Symposium on Plant Growth Modeling, Simulation, Visualization and Applications. Shanghai, Chine (2012)

22. Lowe, D.G.: Distinctive image features from scale-invariant keypoints. International Journal of Computer Vision 60(2), 91–110 (Nov 2004)

23. Meagher, D.: Octree Encoding: a New Technique for the Representation, Manipulation and Display of Arbitrary 3-D Objects by Computer. Electrical and Systems Engineering Department Rensseiaer Polytechnic Institute Image Processing Laboratory (1980)

24. Mendez-Vigo, B., de Andres, M., Ramiro, M., Martinez-Zapater, J., Alonso-Blanco, C.: Temporal analysis of natural variation for the rate of leaf production and its relationship with flowering initiation in arabidopsis thaliana. Journal of Experimental Botany 61(6), 1611–23 (2010)

25. Munns, R., James, R.A., Sirault, X.R.R., Furbank, R.T., Jones, H.G.: New phenotyping methods for screening wheat and barley for beneficial responses to water deficit. Journal of Experimental Botany 61(13), 3499–3507 (Aug 2010)

26. Paproki, A., Sirault, X., Berry, S., Furbank, R., Fripp, J.: A novel mesh processing based technique for 3d plant analysis. BMC Plant Biology 12(1), 63 (2012)

27. Paulus, S., Schumann, H., Kuhlmann, H., Leon, J.: High-precision laser scanning system for capturing 3d plant architecture and analysing growth of cereal plants. Biosystems Engineering 121, 1–11 (May 2014)

28. Pisek, J., Sonnentag, O., Richardson, A.D., Mottus, M.: Is the spherical leaf inclination angle distribution a valid assumption for temperate and boreal broadleaf tree species? Agricultural and Forest Meteorology 169(0), 186 – 194 (2013)

29. Schuchert, T., Scharr, H.: Estimation of 3d object structure, motion and rotation based on 4d affine optical flow using a multi-camera array. In: Proceedings of the 11th European Conference on Computer Vision: Part IV. pp. 596–609. ECCV'10, Springer-Verlag, Berlin, Heidelberg (2010)

30. Snavely, N., Seitz, S.M., Szeliski, R.: Photo tourism: Exploring photo collections in 3d. In: SIGGRAPH Conference Proceedings. pp. 835–846. ACM Press, New York, NY, USA (2006)

31. Steinbruecker, F., Kerl, C., Sturm, J., Cremers, D.: Large-scale multi-resolution surface reconstruction from rgb-d sequences. In: IEEE International Conference on Computer Vision (ICCV). Sydney, Australia (2013)

32. Toeppe, E., Nieuwenhuis, C., Cremers, D.: Volume constraints for single view reconstruction. In: IEEE Conference on Computer Vision and Pattern Recognition (CVPR). Portland, USA (2013)

33. Unger, M., Pock, T., Bischof, H.: Continuous globally optimal image segmentation with local constraints. In: Computer Vision Winter Workshop 2008. Moravske Toplice, Slovenija (Feb 2008)